JOURNAL OF GEOPHYSICAL RESEARCH, VOL. 105, NO. D4, PAGES 5027–5036, FEBRUARY 27, 2000

A simple and efficient method for retrieving surface UV radiation dose rate from satellite

Zhanqing Li, Pucai Wang, and Josef Cihlar
Canada Centre for Remote Sensing, Ottawa

Abstract. A continual trend of ozone depletion has drawn much attention to the biologically harmful UV-B radiation from the Sun reaching the Earth's surface. Satellite remote sensing provides a sole means of monitoring the global distribution of surface UV-B. At present, there are very few inversion algorithms with sufficient accuracy and robustness for operational application. A new algorithm is proposed here to infer surface UV-B irradiance and UV erythemal dose rate from satellite observations. The method is based on a simple model that treats UV radiative transfer in three distinct layers: an absorbing layer of ozone, a scattering layer of molecules, cloud and aerosol particles, and a layer of the Earth's surface. UV-B irradiance and dose rate at the surface are determined by the transmittance of the ozone layer, which can be derived from TOMS total ozone measurements, and the reflectance of the scattering layer, which can be determined from any UV or visible channel outside of ozone absorption bands. The inversion algorithm developed here is very simple (a couple of analytical expressions) and contains a few parameters that can be readily obtained from satellites (except for aerosol variables). The performance of the algorithm is validated against the results of comprehensive radiative transfer modeling using a DISORT-based model. Under a wide range of conditions (clear, cloudy, and turbid atmospheres) the retrieved surface UV-B irradiance and erythemal dose rate from the simple inversion algorithm are nearly as accurate as those calculated from the DISRORT-based model but require much less computation and input data.

1. Introduction

Ultraviolet radiation (UV) is detrimental to various types of organisms, including humans, animals, plants, etc. According to the degree of damage, UV radiation is divided into three bands: UV-A (320–400 nm), UV-B (280–320 nm), and UV-C (100–280 nm). UV-A is the least energetic and may cause suntan, whereas UV-C is the most powerful, which can cause mutations and even death with a small amount of exposure. The damage caused by UV-B is somewhere in between. Until recently, the Earth's atmosphere allowed for some UV-A, a little UV-B, and no UV-C radiation reaching the ground because of the absorption by ozone and other gases (O_2, N_2, etc.). However, the shielding effect of the ozone layer is diminishing due to ozone depletion, and surface-observed UV-B has shown a significant upward trend, as found by *Kerr and McElroy* [1993] in Toronto. Several studies presented in the recent European Conference on UV (ECUV) Radiation (see this issue) indicate that such a trend may continue until early next century when the impact of the Montreal Protocol (on phasing out the use of CFCs and other chemicals that damage the ozone layer), signed in 1987, could be significant enough to counteract or halt the trend.

Concerns about the increase in surface UV-B have spawned immense scientific and societal interest, especially following the discovery of the ozone hole in the Antarctic [*Farman et al*., 1985; *Solomon*, 1988] and the serious ozone decreases in middle and high latitudes [*WMO*, 1989; *Bojkov et al*., 1990; *McPeters et al*., 1996; *Wardle et al*., 1997]. Numerous research and monitoring programs were established at national and international levels. Among the most significant achievements of the past decade was the development of ground-based ozone and UV observation networks. Before the 1980s, few stations conducted regular measurements, but now hundreds of ozone/UV stations are operating around the globe. The data are quality controlled and archived in the World Ozone and Ultraviolet Radiation Data Center of the World Meteorological Organization operated by Environment Canada [*Wardle et al*., 1996]. These are supplemented by many research networks such as the U.S. National Science Foundation (NSF) polar UV Network [*Booth et al*., 1995] and the USDA UV Monitoring Network [*Bigelow et al*., 1998]. The advantages of ground-based sensors are numerous. They provide in situ ground-truth values, are easily calibrated and recalibrated, have a finer spatial and temporal resolution, etc. Notwithstanding, ground-based observation alone is insufficient to address the global ozone/UV problems for its inherent limitations, which include sparse and nonuniform spatial coverage, variable observation standard and quality, and short observation periods for the majority of stations. A combination of ground-based and space-borne UV observation would be ideal to best characterize the spatial and temporal variability of UV.

The above limitations can be overcome or lessened by means of space-borne remote sensing. In contrast to ground observation, satellite provides global complete coverage at a moderate resolution with standard sensors. So far, UV has been observed from space for more than 20 years. Early satellite UV measurements were made by the Backscatter Ultraviolet (BUV) sensor onboard the Nimbus 4, which was launched in 1970 and continued functioning for several years [*Stolarski et al*., 1997].

Published in 2000 by the American Geophysical Union.

Paper number 1999JD900124.

Nimbus 7 provided the longest high-quality UV space-borne observation from 1978 to 1993 with the total ozone mapping spectrometer (TOMS). NOAA weather satellites also measured UV radiances for a considerable period with the solar backscatter ultraviolet (SBUV) sensor. TOMS was designed mainly for determining the vertically integrated ozone amount, while SBUV was designed for obtaining ozone profiles. These data are invaluable for studying both ozone [*Reinsel et al*., 1988; *Herman and Larko*, 1994] and surface UV radiation [*Lubin and Frederick*, 1989; *Herman et al*., 1996]. In addition to the Nimbus 7, TOMS instrument was also flown on the Russian Meteor 3 from 1991 to 1994, on the Japanese ADEOS for less than a year in 1996–1997, and currently on the NASA's Earth Probe. Ozone data have also been derived from the TIROS operational vertical sounder (TOVS), the Stratospheric Aerosol and Gas Experiment (SAGE and SAGE II), the Global Ozone Monitoring Experiment (GOME) onboard the European ERS-2 satellite, etc. Together, these satellites provide a wealth of data regarding ozone and UV radiation. More information on the space programs related to ozone and UV observation may be obtained from http://jwocky.gsfc.nasa.gov/.

It is important to note that satellite sensors do not provide direct measurements of ozone and UV. Rather, these quantities are estimated from reflected radiances measured at the top of the atmosphere (TOA) in several narrow spectral regions. The estimation requires inversion algorithms that use satellite measurements as input parameters, together with ancillary information about atmospheric and surface conditions. As such, the accuracy of the retrievals depends both on the inversion algorithms and the input data. As far as the estimation of surface UV radiation is concerned, only a few algorithms have been proposed in two general categories. The first one is based on detailed radiative transfer models, often the relatively fast two-stream codes, with some critical input parameters such as cloud optical depth and ozone amount derived from satellite [*Frederick and Lubin*, 1988; *Madronich*, 1992; *Lubin and Jensen*, 1995; *Qu*, 1997]. The second type is a parameterization scheme which requires fewer parameters [*Eck et al*., 1995; *Krotkov et al*., 1998]. The methods of the first type are, in principle, more accurate if all input variables are known accurately. In practice, this is unfortunately not the case. Often, information on input variables is highly limited and inaccurate. Furthermore, the heavy computation burden is another major obstacle confronting the processing of global satellite data. While the second method is more practical and feasible for operational application, the accuracy of retrieval may be limited by the assumptions and empirical coefficients involved in the development of the parameterization [*Eck et al*., 1995].

In this study, we propose an alternative parameterization algorithm with fewer assumptions and empirical coefficients. The algorithm is based on a simplified radiative transfer model with most model parameters determined physically. The performance of the algorithm is tested against the results of computations with a detailed radiative transfer model. The framework and concepts in the design of UV-B inversion algorithm are similar to those for retrieving surface broadband solar radiation budget [*Li et al*., 1993] and surface photosynthetically active radiation [*Li and Moreau*, 1996]. However, differences are numerous due to different radiative transfer processes and radiative quantities.

The following section describes a detailed radiative transfer model used as a tool in this study and discusses some sensitivity test results obtained from the model, which help the development of the inversion algorithm. Section 3 is the core of the paper that provides a detailed description and derivation of the inversion algorithm. The performance of the algorithm is assessed in section 4 by comparing results from the inversion algorithm with those from the detailed radiative transfer model.

2. Radiative Transfer Modeling

While the inversion algorithm to be designed is not based on a detailed radiative transfer model, the latter is instrumental in understanding the physics behind the inversion. The popular discrete ordinate method (DISORT) was adopted in this study. The DISORT method was first proposed by *Chandrasekhar* [1950] and later modified and improved by *Liou* [1973] and *Stamnes et al*. [1988]. Following successful applications in modeling the UV transfer by *Stamnes et al*. [1990, 1991], *Tsay and Stamnes* [1992], the DISORT method has been employed most widely for UV studies [*Zeng et al*., 1994; *Wang and Lenoble*, 1994; *Forster*, 1995; *Forster et al*., 1995; and many others as presented in the recent ECUV, this issue].

The detailed model employed in this study was developed by *Wang and Lenoble* [1994], based on the DISORT method [*Stamnes et al*., 1988]. The model was demonstrated to be accurate in comparison with ground observations [*Wang and Lenoble*, 1994]. The model assumes a plane-parallel layered atmosphere with 20 homogeneous layers. The layers are very thin in the lower atmosphere (as thin as 200 m) and thick (more than 5 km) in the upper atmosphere.

The extraterrestrial solar spectral irradiance data were taken from the WMO report [*Fröhlich and London*, 1986]. Data on ozone absorption cross sections were obtained from *Molina and Molina* [1986] for three temperatures: 226, 260, and 298 K. The values for other temperatures were derived by linear interpolation. Aerosol models were adopted from LOWTRAN 7 [*Kneizys*, 1988]. These models specify the different vertical distributions and the wavelength dependence of the aerosol extinction coefficients and single-scattering albedo. Aerosol asymmetry factor was treated as constant in the UV-B range. *Wang and Lenoble* [1994] incorporated 10 types of cloud defined by *Falcone* [1979] into their model. These clouds differ primarily in phase and microphysics. The size distribution of the cloud droplets is given by a modified Gamma function. Using these, cloud optical properties were determined following Mie calculations. The results indicate that the UV extinction coefficients for all the cloud models have almost the same wavelength dependence. The cloud asymmetry factors vary only slightly, from 0.79 to 0.82. The single-scattering albedos of all the cloud models are essentially equal to 1, implying no cloud absorption. Therefore as far as UV modeling is concerned, differences due to cloud types are minimal, as was noted also by *Forster* [1995]. The fundamental cloud variable is cloud optical thickness.

The DISORT-based model was first employed for conducting sensitivity tests. Although many sensitivity studies have been reported [*Zeng et al*., 1994; *Wang and Lenoble*, 1994; *Forster*, 1995], they are concerned with surface UV-B only. The emphasis of our sensitivity study is on the understanding of the relationship between satellite-observed and surface-inferred quantities, as the essence of developing an inversion algorithm is to establish the relation. The sensitivity tests are proven to be instrumental in developing the inversion algorithm. Instead of showing downward UV irradiance as is usually the case, sur-

face-absorbed UV irradiance (or net UV) is presented and discussed throughout the paper. With the knowledge of surface UV albedo, the two quantities are fully interchangeable. As in other retrieving methods, surface UV albedo is treated as a known input variable.

Figure 1 shows the sensitivity to cloud optical depth of the UV-B irradiance absorbed at the surface (or surface net UV-B) and TOA albedo (the ratio of upwelling and downwelling irradiances) at 360 nm. The former is a quantity to be inferred, while the TOA albedo can be measured by TOMS and used as a major input variable in the inversion (compare later discussions for reasoning). It is evident that surface UV-B is very sensitive to cloud optical depth. For a thin cloud of optical thickness 10, surface net UV-B irradiance is only about half the amount of its clear-sky value, although the sensitivity diminishes quickly as cloud becomes thicker. It is because of the strong sensitivity that effort and precision in the retrieval of surface UV-B following the first approach were dictated largely by the retrieval of cloud optical depth [e.g., *Frederick and Lubin*, 1988; *Qu*, 1997]. Accompanied with the change in surface UV-B is the variation in top of atmosphere (TOA) albedo (Figure 1b). The trends of variation in the two quantities are opposite; that is, a monotonous decrease in surface UV-B irradiance is associated with a monotonous increase in TOA UV albedo at 360 nm. Such a coupling relation is totally understandable, as cloud enhances TOA reflection and reduces atmospheric UV transmission. Since 360 nm is outside of the ozone absorption band, reflection at this wavelength can serve as a good proxy of cloudiness. One may thus take advantage of the relation between the TOA and the surface quantities to circumvent the need for cloud optical depth in retrieving net surface UV-B irradiance.

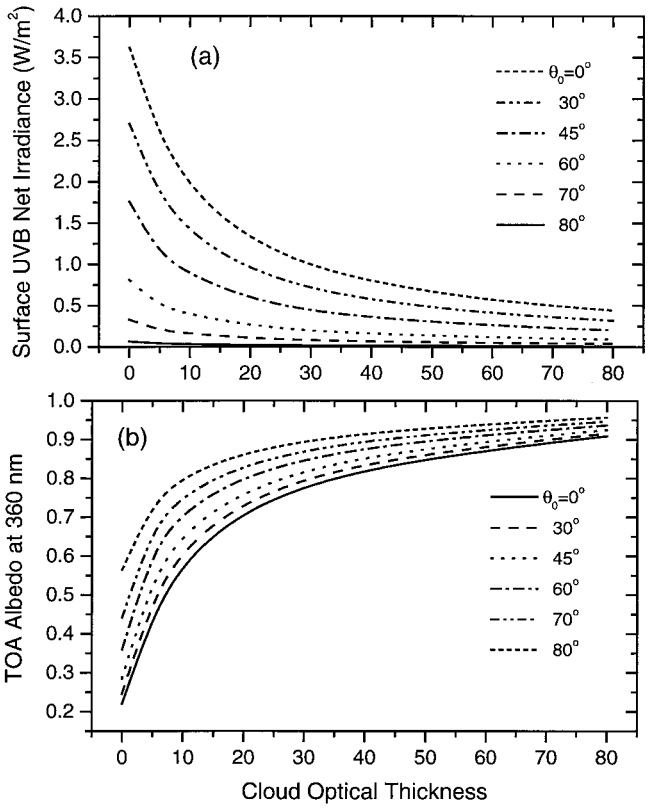

Figure 1. Variations of (a) UV-B irradiance absorbed at the Earth's surface and (b) TOA albedo at 360 nm with cloud optical thickness at various solar zenith angles (θ_0). The simulations are for the U.S. Standard Atmosphere with a total ozone amount of 343 DU and a cloud between 1 and 2 km.

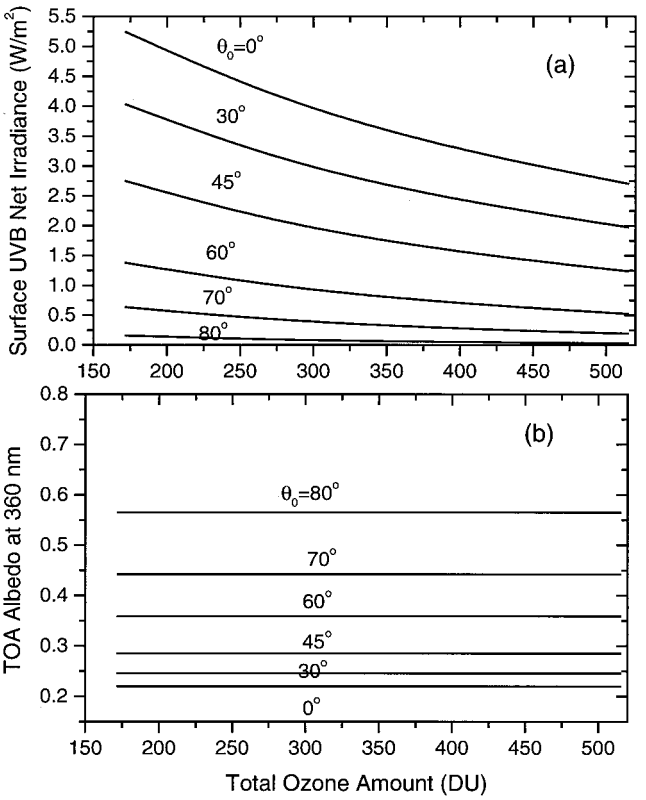

Figure 2. Same as Figure 1 but with total ozone amount without any cloud and aerosol.

The sensitivity of the same surface and TOA quantities to total ozone content are presented in Figure 2. It is seen that surface UV-B decreases significantly with increasing ozone amount at a more stable rate than its decrease with cloud optical depth. However, TOA albedo remains constant, because of the lack of absorption by ozone at 360 nm. On the other hand, TOA albedo in an ozone absorption band decreases as ozone amount increases. This suggests that measurements made in ozone sensitive band would be needed to account for the effect of ozone on surface UV-B. However, since ozone amount has been retrieved rather accurately from satellite [*Herman et al.*, 1994; *McPeters et al.*, 1996], it can be treated as a known input variable.

Figure 3 shows the sensitivity results for two types of aerosols, a weakly absorbing maritime aerosol (dashed lines) and a moderately absorbing continently aerosol (solid line) with single-scattering albedos of 0.98 and 0.95, respectively, as defined in *WCP* [1986]. Although the range of the changes at both the surface and the TOA is small due to the low aerosol optical depth, the variations are similar to those due to cloud. In fact, for completely nonabsorbing aerosols, the effects of aerosol optical depth are identical to those of cloud optical depth. For absorbing or relatively absorbing aerosols, larger variations are observed at the surface than at the TOA. This is because absorbing aerosols impede transmission more than reflection.

The effects of surface albedo are presented in Figure 4. As for cloud, both quantities are very sensitive to surface albedo.

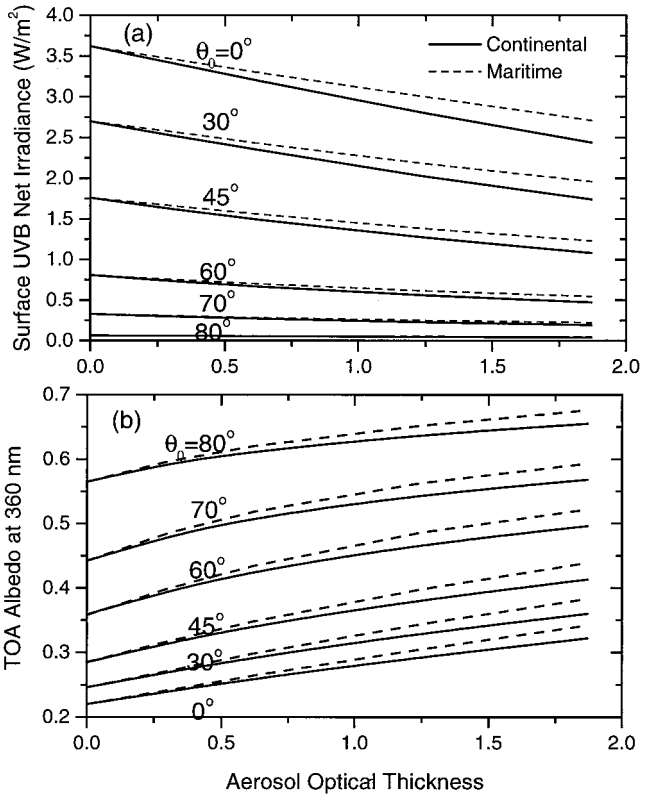

Figure 3. Same as Figure 1 but without cloud and with varying aerosol optical thickness for two types of aerosols: the moderately absorbing continental aerosol ($\omega_0 = 0.95$) (solid line) and the weakly absorbing aerosol ($\omega_0 = 0.98$) (dash line).

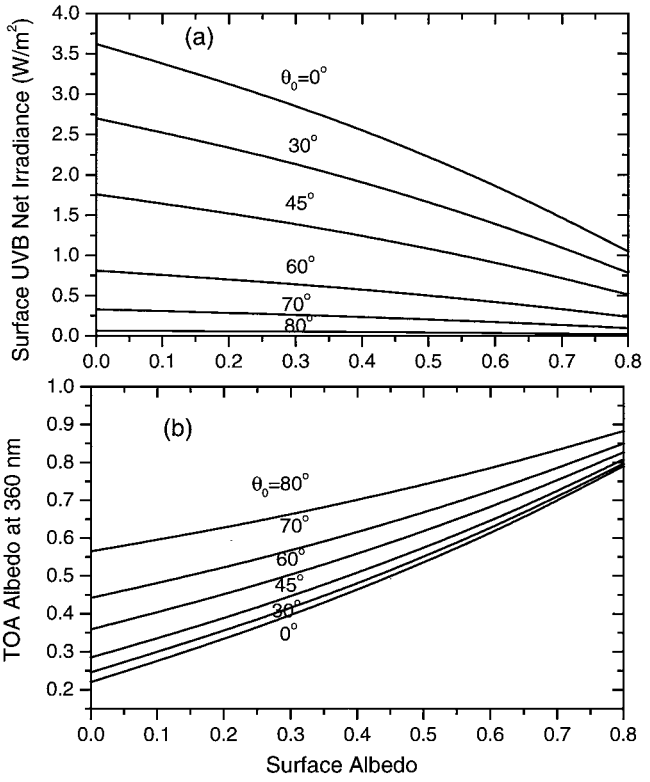

Figure 4. Same as Figure 1 but without cloud and with varying surface albedo.

If Figure 1 were shown in terms of cloud top albedo in lieu of cloud optical depth, the curves would be almost identical to those for surface albedo under the same atmospheric conditions without any absorbing aerosols. This finding is important for the inversion, as it suggests that no differentiation is required between cloud and surface albedo. Albedo is, however, needed to convert surface net UV-B into downward UV-B. The effects of other variables (such as ozone and aerosol profile, cloud position) are generally much smaller [*Wang and Lenoble*, 1994; *Forster*, 1995]. Given that these parameters are often unavailable, the inversion algorithm does not include them.

3. Development of the Inversion Algorithm

The inversion algorithm proposed here was built on a simple conceptual UV transfer model, as is illustrated in Figure 5. In essence, the UV radiative transfer processes taking place in the atmospheric column are simplified into three distinct layers. The first layer accommodates ozone in the upper atmosphere whose density is typically highest in the lower stratosphere (20–25 km). The second layer contains an ensemble of atmospheric molecules, cloud, and aerosol particles. The third layer is the surface. As is seen from Figure 5, the photons first enter the ozone layer and some are absorbed due to ozone absorption. In reality, a small fraction of photons may be scattered back to space by a thin layer of the atmosphere in and above the ozone layer. Such an effect is taken into account collectively with other scattering media contained in the second layer. In addition to the dominant scattering events, the UV photons reaching this layer may be subject to further absorption due to the existence of absorbing aerosols. Most of the UV photons transmitted through the second layer are absorbed at the surface, since UV albedo is very low (0.01–0.1) for the majority of surface types except for snow/ice [*Eck et al.*, 1987; *Blumthaler and Ambach*, 1988]. The reflected photons as measured by satellite consist of those scattered upward by atmo-

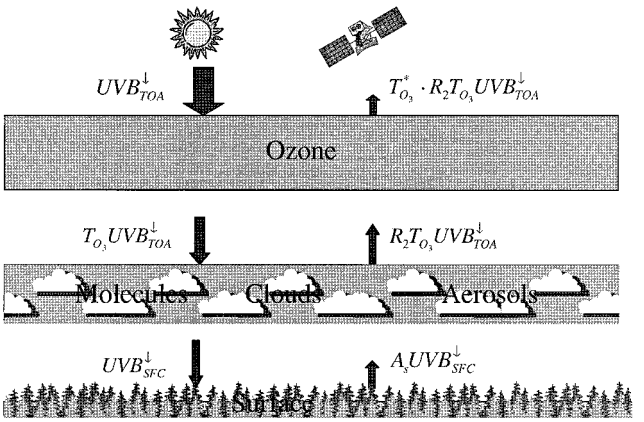

$$UVB_{SFC} = (1-R_2)T_{O_3}UVB^{\downarrow}_{TOA} - \Delta UVB_{ATM}$$

$$\Delta UVB_{ATM} = A_2 T_{O_3} UVB^{\downarrow}_{TOA} + A^{*}_{2} A_s UVB^{\downarrow}_{SFC}$$

Figure 5. A schematic of a simple radiative transfer model for the development of a surface UV-B inversion algorithm. The atmospheric column is divided into three distinct layers: the top layer containing ozone only, the middle layer including atmospheric molecules and cloud and aerosol particles, and the third layer being the surface.

spheric molecules, cloud and aerosol particles and the surface, and not absorbed by the ozone layer.

An UV-B inversion algorithm is concerned essentially with the linkage between two quantities: TOA-reflected irradiance in UV-B ($UVB^{\uparrow}_{TOA}$) or other bands of satellite sensors as specified later, and surface downwelling UV-B ($UVB^{\downarrow}_{SFC}$). Note that a scanning radiometer can only measure reflected radiance; irradiance may be inferred from radiance by means of BRDF correction. To establish the linkage, we may start simply from the energy conservation law. Let UVB_{SFC}, $UVB^{\downarrow}_{TOA}$, and UVB_{ATM} denote the UV-B fluxes absorbed at the surface, incident at the TOA and absorbed in the atmospheric column, respectively. Then we have

$$UVB_{SFC} = UVB^{\downarrow}_{TOA} - UVB^{\uparrow}_{TOA} - UVB_{ATM}, \tag{1}$$

where $UVB^{\downarrow}_{TOA}$ can be calculated from the Sun-Earth distance (d), cosine of the solar zenith angle μ_0, and the extraterrestrial solar UVB spectrum $S(\lambda)$:

$$UVB^{\downarrow}_{TOA} = \frac{\mu_0}{d^2}\int_{280}^{320} S(\lambda)\, d\lambda \tag{2}$$

The attenuation of the incident TOA UV-B caused by ozone absorption is characterized by an ozone transmission function T_{O_3} for downwelling direct UV-B beam. UV-B irradiance transmitted through the layer is given by $UVB^{\downarrow}_{TOA}\, T_{O_3}$, which is then reflected in the two layers beneath the ozone layer due to various scattering events caused by atmospheric molecules, cloud and aerosol particles, and the Earth's surface. The amount of reflection is governed by the UV-B albedo (R_2) in the column composed of layers 2 and 3, i.e., $R_2 UVB^{\downarrow}_{TOA}\, T_{O_3}$. The reflected diffuse UV-B photons travel through the ozone layer and some are absorbed again. The absorption rate is determined by ozone transmittance for diffuse radiation, $T^*_{O_3}$. Considering all these events, $UVB^{\uparrow}_{TOA}$ can be expressed as

$$UVB^{\uparrow}_{TOA} = R_2 T_{O_3} T^*_{O_3} UVB^{\downarrow}_{TOA} \tag{3}$$

To determine UVB_{ATM}, we first consider a simple case without any absorbing aerosols. UV atmospheric absorption is then entirely due to ozone that absorbs UV-B photons coming both from above and below the ozone layer with absorption rates given by $(1 - T_{O_3})$ and $(1 - T^*_{O_3})$, respectively. The total absorption is therefore given by

$$UVB_{ATM} = [(1 - T_{O_3}) + T_{O_3} R_2 (1 - T^*_{O_3})] UVB^{\downarrow}_{TOA}. \tag{4}$$

Combining (1), (3), and (4) leads to a simple relation between R_2 and UVB_{SFC}:

$$UVB_{SFC} = (1 - R_2) T_{O_3} UVB^{\downarrow}_{TOA}. \tag{5}$$

With the presence of absorbing aerosols, an additional absorption term needs to be included in (5), so

$$UVB_{SFC} = (1 - R_2) T_{O_3} UVB^{\downarrow}_{TOA} - \Delta UVB_{ATM}. \tag{6}$$

Similar to ozone absorption, the additional absorption due to aerosol is determined by downward and upward UV-B irradiances above and below the aerosol layer (layer 2) and the corresponding aerosol absorption coefficients. The two irradiance components are given by $T_{O_3} UVB^{\downarrow}_{TOA}$ and $A_s UVB^{\downarrow}_{SFC}$, respectively, where A_s denotes surface albedo. The aerosol absorption coefficients are parameterized following the format of the Beer's law which is, strictly speaking, valid for direct monochromatic solar beam only:

$$A_2 = 1 - \exp(-a_2 \tau_a), \tag{7}$$

$$A^*_2 = 1 - \exp(-b_2 \tau_a), \tag{8}$$

where A_2 and A^*_2 denote absorptance for downward and upward UV radiation due to aerosol absorption; τ_a is aerosol-absorbing optical depth that is related to aerosol total optical depth τ_e through aerosol single-scattering albedo ω_0,

$$\tau_a = (1 - \omega_0)\tau_e \tag{9}$$

It follows from these equations that the additional term vanishes for a conservative aerosol ($\omega_0 = 1$). Values a_2 and b_2 are atmospheric amplification factors for downward and upward UV irradiances, respectively. For the upward diffuse UV-B radiation, b_2 is equal to the diffusivity factor (1.66). Determination of the amplification factor for downward radiation is more complex, depending on sky condition and cloud height relative to the aerosol layer. For a plane-parallel atmosphere it is equal to the inverse of the cosine of the solar zenith angle (μ_0) under clear-sky conditions. Under cloudy skies, if the aerosol layer is below the bulk of cloud, it should be set to the diffusivity factor as well. For other intermediate conditions, its value is somewhere in between. In practice, it is difficult to determine the exact value, since there is scarcity of information on aerosol vertical distribution relative to the cloud position. Therefore a constant value of 1.33 is recommended for general use that was determined from simulation results for a great variety of atmospheric conditions, as discussed in the following section:

The additional absorption due to aerosol can thus be expressed as

$$\Delta UVB_{ATM} = A_2 T_{O_3} UVB^{\downarrow}_{TOA} + A^*_2 A_s UVB^{\downarrow}_{SFC}. \tag{10}$$

Noting that that downward surface UVB is equal to the net surface UVB divided by $(1 - A_s)$, we can derive an expression for UVB_{SFC} from (6) and (10), of a similar format to (5) for a turbid atmosphere with absorbing aerosols:

$$UVB_{SFC} = [(1 - R_2) - A_2] C T_{O_3} UVB^{\downarrow}_{TOA} \tag{11}$$

where

$$C = \frac{(1 - A_s)}{(1 - A_s) + A^*_2 A_s}. \tag{12}$$

It is clear from the comparison between (5) and (11) that the effect of absorbing aerosol is represented by two coefficients, namely A_2 and C. Note that the coefficient C is generally very close to unity, since UV-B surface albedo is very small. For a grassland, for example, it is as small as 0.01 [*Blumthaler and Ambach*, 1988]. Besides, the absorptance for upwelling diffuse UV-B denoted by A^*_2 is also usually a very small number, leading to an almost negligible product, $A^*_2 A_s$. Therefore the major factor correcting the influence of absorbing aerosol is A_2 in (11).

Note that R_2 represents UV-B albedo for the entire atmospheric column without ozone absorption. Although TOMS has two channels in the UV-B band at 312 and 317 nm, their measurements do not represent R_2 for two reasons. First, the measurements only sample a very small fraction of the UV-B region (the bandwidth is nominally 1 nm). Second and more importantly, they are contaminated by ozone absorption. For the second reason, R_2 is better derived from measurements made outside of the ozone absorption bands, such as the TOMS 360 nm or 380 nm channels. The spectral variation of

Table 1. Fitted Ozone Effective Absorption Coefficients and Their Corresponding Weighting Factors

Interval, nm	k_{eff}	W_i
280–290	42.46	0.139
290–300	14.52	0.257
300–310	4.37	0.268
310–315	1.69	0.162
315–320	0.863	0.174

upwelling UV can be accounted for based on modeling or observation [*McKenzie et al*., 1996]. It is even more advantageous to derive R_2 from visible measurements, since there are plenty of visible satellite data available from operational weather satellites such as NOAA/AVHRR and GOES, provided that R_2 is well correlated with the visible albedos. In addition to the long history of observation, geostationary satellites have an important unique feature that they provide measurements of high temporal frequency to allow a diurnal sampling.

Extensive radiative transfer modeling for a variety of conditions (compare section 4) indicate that R_2 is highly correlated with albedo measurements in TOMS 360 nm channel, R_{360}, by a linear relationship:

$$R_2 = a + bR_{360} \tag{13}$$

where the coefficients a and b were determined to be $a = 0.196$, $b = 0.798$. The same modeling results indicate that R_{360} can be estimated from NOAA/AVHRR visible channel with high accuracy by the following equation:

$$R_{360} = 0.394 - 0.217\mu_0 + (0.684 + 0.173\mu_0)R_{\text{VIS}} \tag{14}$$

The UV-B band mean transmittance due to ozone absorption T_{O_3} is also computed by an efficient parameterization scheme, as proposed by *Chou* [1996]. The scheme consists of a series of exponential functions. Each function corresponds to an UV-B subinterval within which a constant effective ozone absorption coefficient (k_i) is assumed. The function is weighted by the proportion of the solar energy falling within the subinterval, relative to total UV-B irradiance incident at the TOA (W_i):

$$T_{O_3} = \sum_{i=1}^{n} W_i \exp(-k_i u/\mu_0), \tag{15}$$

where u is total ozone amount in centimeters. The ozone effective absorption coefficient in a subinterval is determined by the following equations:

$$k_i = -(\ln T_i)/(u/\mu_0). \tag{16}$$

$$T_i = \frac{1}{S_i}\int_{\Delta\lambda} S(\lambda)\exp\left[-k(\lambda)\frac{u}{\mu_0}\right] d\lambda \tag{17}$$

$$S_i = \int_{\Delta\lambda} S(\lambda)\, d\lambda \tag{18}$$

where T_i represents band mean ozone transmittance integrated over the subinterval i. $S(\lambda)$ and S_i denote TOA solar spectral irradiances at wavelength λ and over the subinterval i, respectively.

Table 1 gives the spectral intervals, effective absorption coefficients, and weighting factors for computing UV-B ozone band mean transmittance derived from the above equations. Because of the dramatic fluctuation in the ozone cross section with wavelength, the effective absorption coefficients differ by 2 orders of magnitude among the five selected intervals. The transmittance computed using the parameterization is accurate to within 0.02 for total ozone amount ranging from 172 to 515 Dobson units (DU) and solar zenith angle from 0° to 80°.

Note that both the principles and the format of the inversion algorithm for retrieving UV-B irradiance are totally applicable to the retrieval of surface monochromatic UV irradiance and biologically active UV irradiance (BUV_{SFC}) defined by

$$\text{BUV} = \int_{280}^{400} f(\lambda)A(\lambda)\, d\lambda \tag{19}$$

where $f(\lambda)$ represents UV spectral irradiance reaching the Earth's surface, $A(\lambda)$ is a spectral weighting function or an action spectrum for the biological process of interest [*Madronich*, 1992]. While there are many types of UV dose rates measuring, for example, erythema induction, generalized DNA damage, and generalized plant damage, the most widely used is the erythemal UV (EUV) radiation. Basically, the formulae for retrieving UV-B hold for EUV except that all spectrally integrated quantities need to be weighted by the action spectrum. For example, the ozone band-mean transmittance is defined by

$$T_{O_3,\text{eff}}^{\text{EUV}} = \int_{280}^{400} T_{O_3}(\lambda)S(\lambda)A(\lambda)\, d\lambda \Big/ \int_{280}^{400} S(\lambda)A(\lambda)\, d\lambda, \tag{20}$$

Following the same procedure as for computing UV-B ozone transmittance, $T_{O_3,\text{eff}}^{\text{EUV}}$ is also calculated by (15) but with different sets of coefficients given in Table 2. Comparing Tables 1 and 2, one may note that the weighting coefficients in the first two bands increased considerably because the action spectrum is heavily weighted toward the short wavelengths [*Madronich*, 1992]. Other changes for retrieving EUV include modified coefficients in (7) and (8): $a_2 = 1.15$, $b_2 = 1.66$; and in (13), $a = 0.193$, $b = 0.817$.

4. Validation of the Inversion Algorithm Against Modeling Results

Equation (11), the linear relationship between surface UV-B net irradiance and satellite-measured TOA albedo, is the core of the inversion algorithm. Since no assumptions and empirical tuning are involved in formulating the algorithm, it should be applicable to any combination of atmospheric, cloud, and surface conditions. However, the use of such an extremely sim-

Table 2. Same as Table 1 but for Computing EUV Ozone Transmittance

Interval, nm	k_{eff}	W_i
280–290	42.460	0.3055
290–300	18.625	0.5424
300–310	5.460	0.1292
310–315	1.418	0.0124
315–320	0.531	0.0043

plified radiative transfer model warrants a thorough evaluation of the validity and precision of the algorithm. A straightforward test is to compare the outputs of the inversion algorithm with those from a detailed radiative transfer model. To this end, we carried out extensive radiative transfer calculations with the DISORT-based model as described earlier.

The first test is to verify the basis of (11). Figure 6 presents a series of plots delineating the impact of cloud, ozone, aerosol, and surface albedo on the relationship between UVB_{SFC} and R_{360}. The four panels (Figures 6a, 6b, 6c, and 6d) correspond to Figures 1, 2, 3, and 4, respectively. It is seen clearly that for fixed solar zenith angles the two variables are indeed linearly correlated. The relationship is formed by changing cloud optical depth (Figures 6a–6c) as well as surface albedo (Figure 6d). Therefore the relationship can be used to infer surface UV-B irradiance from satellite-measured TOA albedo without the knowledge of cloud optical thickness. This avoids a major source of uncertainty. The relationship is, however, altered considerable by ozone amount in terms of both slope and intercept, as is shown in Figure 6b. For a given TOA albedo, surface net UV-B irradiance may differ by a factor of 2 as the total ozone amount ranges from 172 to 515 DU. The influence of ozone is easily understood from (5), which includes a term of ozone transmittance. Figure 6c shows the effect of aerosol for a moderately absorbing continental aerosol. As mentioned earlier, conservative aerosol has no effect on the relation, which is confirmed by detailed radiative transfer modeling (not shown here). The aerosol modifies the intercept substantially but has little impact on the slope. This can also be understood with reference to (11). As discussed earlier, among the two aerosol terms, the offset A_2 is much larger than the slope C. Figure 6d shows the effect of surface albedo. Although changes in albedo modify both the surface and the TOA quantities, they do not distort their relationship. Basically, they cause changes along the same line as that formed by the changes in cloud optical depth. Therefore the retrieval of surface net UV-B does not need the input of surface albedo; however, surface albedo is needed to obtain downwelling UV-B from net UV-B. Together, the results shown in Figure 6 strongly support the fundamentals of the simple UV-B radiative transfer model as delineated in Figure 5.

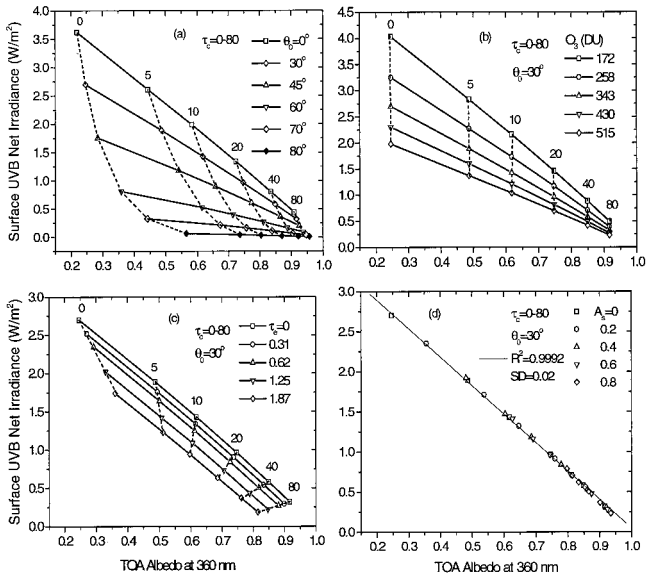

Figure 6. Relationships between the UV-B irradiances absorbed at the surface and reflected at the TOA due to changes in cloud optical depth, and in (a) SZA, (b) ozone amount, (c) aerosol optical depth, and (d) surface albedo. The atmospheric conditions for simulating the results shown in Figures 6a–6d are the same as those shown in Figures 1, 2, 3, and 4, respectively.

Table 3. Specification of Input Parameters and Their Values for DISORT Modeling

Input Parameters	Values
Solar zenith angle	0°, 30°, 45°, 60°, 70°, 80°
Surface albedo	0, 0.2, 0.4, 0.6, 0.8
Ozone amount, DU	172, 258, 343, 430, 515
Cloud optical depth	0, 5, 10, 20, 40, 80
Aerosol optical depth	0, 0.31, 0.62, 1.25, 1.87
Aerosol single-scattering albedo	0.85, 0.90, 0.95, 0.98

The accuracy of the inversion algorithm was assessed by the following procedure: First, radiative transfer calculations were conducted with the DISORT-based model for a large range of atmospheric, cloud, and surface conditions. Second, the inversion algorithm was applied to the simulated satellite TOA albedos, together with total ozone amount and aerosol data (optical depth and single-scattering albedo) to estimate surface UV-B. Third, the estimated surface UV-B irradiances were compared with those computed from the DISORT-based model.

Table 3 lists the input parameters and their values adopted in the simulations. They cover a wide variety of conditions that

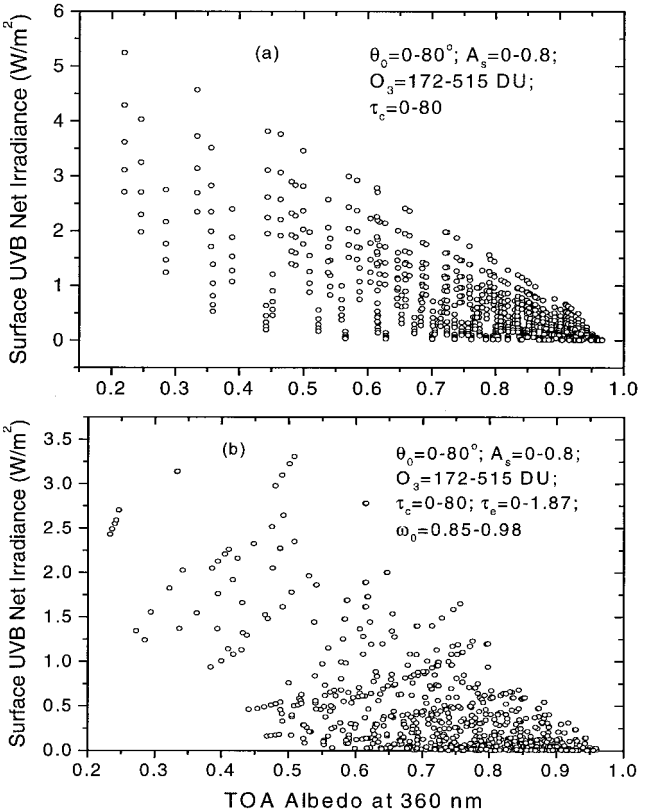

Figure 7. Variations in surface net UV-B irradiance resulting from the selection of a variety of atmospheric, cloud, and surface conditions as delineated in Table 2 for (a) aerosol free and (b) aerosol-loading conditions.

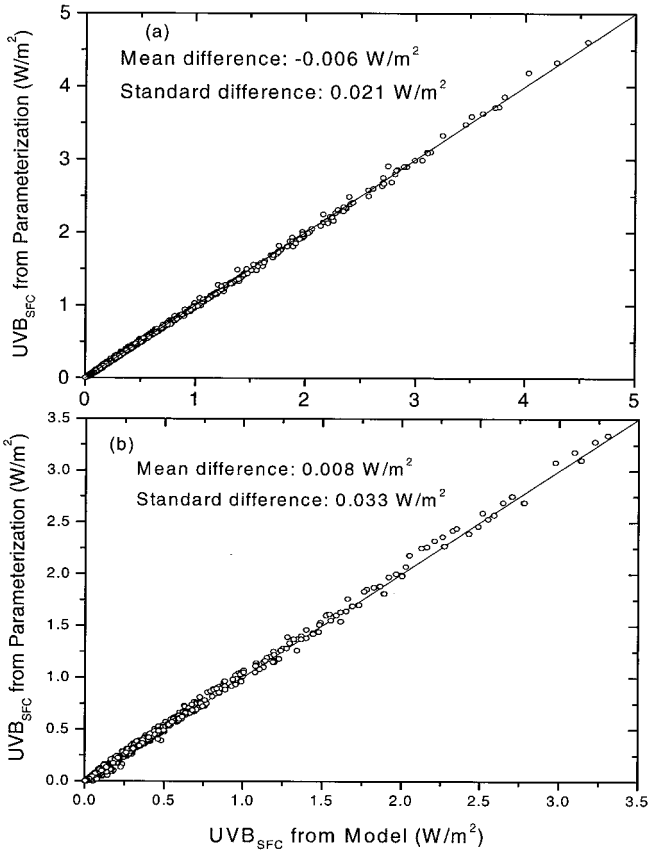

Figure 8. Comparisons of surface net UV-B irradiances estimated from the inversion algorithm and obtained from modeling with a DISORT-based model for (a) aerosol free and (b) aerosol-loading cases shown in Figure 7 and Table 2.

may occur in reality. Consequently, the simulated TOA and surface irradiances vary over a very large range, as is shown in Figure 7 for two categories: without and with aerosols. The results of comparison are presented in Figure 8. The agreement is remarkable for both categories. The mean differences are nearly zero, and the standard deviation is very small. The results of comparisons for erythemal UV dose rate (Figure 9) are also good. Given the extreme simplicity of the inversion algorithm, the high accuracy in reproducing the results of a much more complex model shows its great potential for operational application in the remote sensing of surface UV-B.

The loss of accuracy due to the use of the simple inversion algorithm relative to the complex DISORT model is much smaller than the combination of uncertainties in both model and input parameters. *Schwander et al*. [1997] investigated uncertainties in modeled surface UV irradiances due to various input parameters. The mean relative uncertainty is 5% under clear-sky conditions. It increases to 10–15% without the measurements of aerosol-absorbing properties except for aerosol loading. As explained earlier, aerosol single-scattering albedo is the most uncertain input variable in the retrieval of surface UV-B. Its strong influence is demonstrated in Figure 10 which presents the same comparison as Figures 8b and 9b but assuming $\omega_0 = 1$ for all cases. The agreement deteriorated dramatically. While the results are somewhat exaggerated by the inclusion of some heavy aerosol loadings in the calculation, the strong dependence of the accuracy in the retrievals of UV-B on the specification of aerosol properties is clearly seen, as was also found by *Krotokov et al*. [1998]. It is worth noting that a major progress made recently toward the characterization of absorbing aerosol using TOMS data [*Hsu et al*., 1996; *Herman et al*., 1997]. There will be a wealth of information on aerosol optical depth available from a suite of sensors in the Earth observation system [*King et al*., 1992]. Therefore the inclusion of aerosol optical properties in the current inversion algorithm is, in particular, important and necessary for future applications.

5. Summary

A potential increase in the harmful ultraviolet radiation reaching the Earth's surface has been a major environmental concern since the discovery of the ozone hole in the Antarctic. Much effort has been made to monitor the spatial distributions and temporal trends of ozone and UV radiation to study their relationship. While many observing stations were installed in the past decade, the UV networks is far from being adequate in terms of their spatial coverage, temporal continuity, and observation standard. Satellite-based remote sensing offers some unique advantages over the ground-based observation, such as, global and uniform coverage, long-term and continuous observation, etc.

Inversion algorithms are required to convert satellite measurements of reflected radiance at the TOA to the UV-B irradiance reaching the Earth's surface. While one may resort

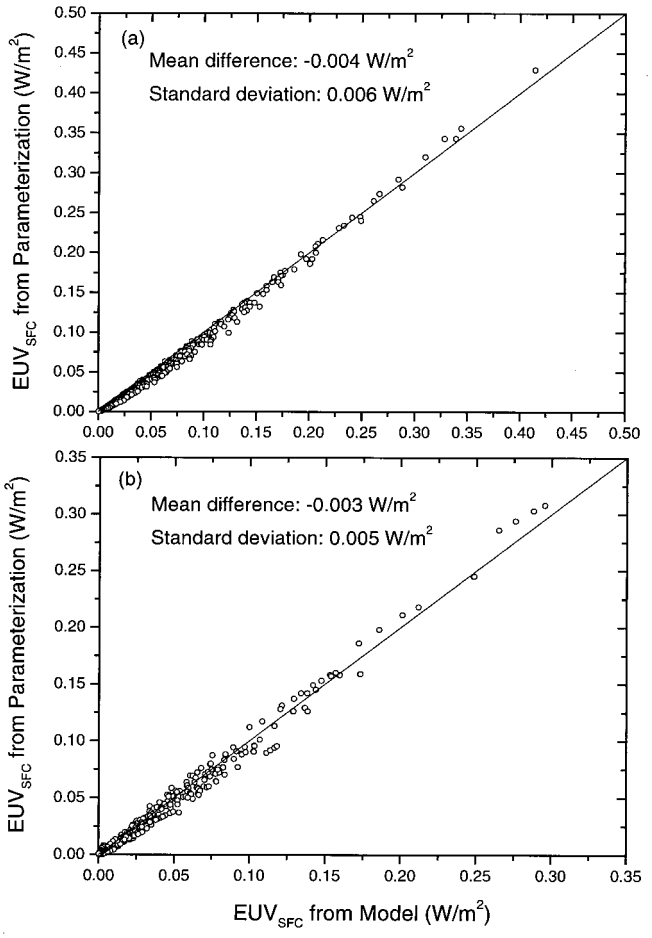

Figure 9. Same as Figure 8 but for EUV.

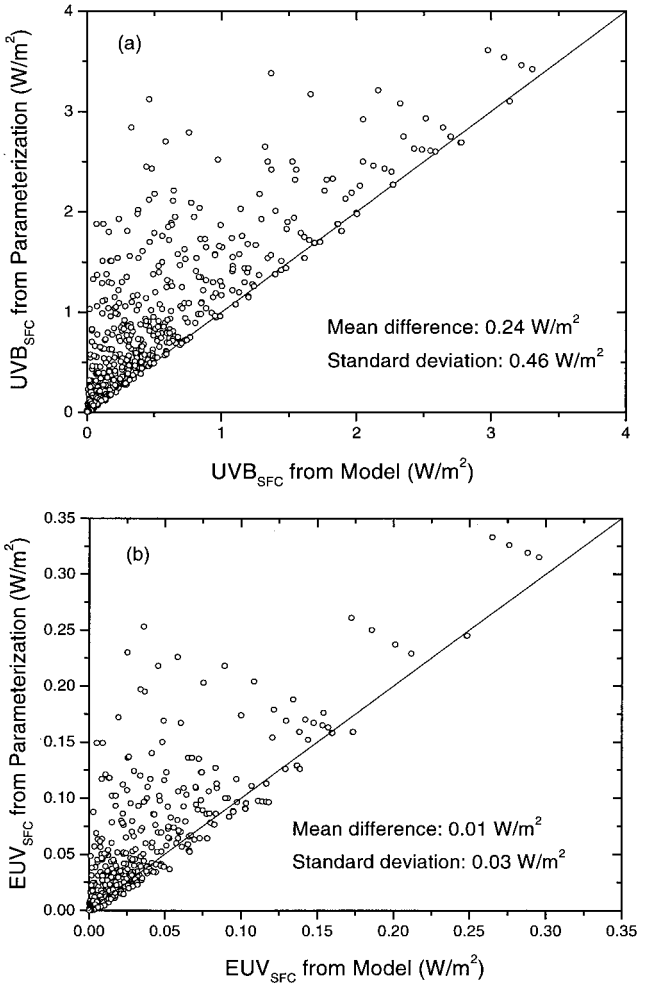

Figure 10. (a, b) Same comparisons as in Figures 8 and 9, respectively but without the correction of aerosol effect in the inversion.

to a detailed radiative transfer model for the conversion, the approach suffers from shortcomings of high computation burden and lack of information on model input parameters. A more feasible approach for operational application is to use a simple algorithm with few parameters that are readily available. Following this philosophy, we proposed a parameterized algorithm based on a simplified radiative model. The algorithm consists of only a couple of equations with four input variables, namely, the TOA UV or visible albedo, total ozone amount, solar zenith angle, and aerosol properties. Except for aerosol, the input variables are available with good accuracy. Since the algorithm was derived with few assumptions and empirical parameters, the algorithm is valid in principle to any conditions. In virtue of comparison with the results of extensive modeling using a detailed DISORT-based radiative transfer model, the simple inversion algorithm is found to be able to estimate surface UV-B irradiance very accurately, under a wide variety of conditions. The algorithm is also tested against real observational data, and the results are also very encouraging [*Wang et al*., this issue].

References

Bigelow, D. S., J. R. Slusser, A. F. Beaubien, and J. H. Gibson, The USDA ultraviolet radiation monitoring program, *Bull. Am. Meteorol. Soc*., *79*, 601–615, 1988.

Blumthaler, M., and W. Ambach, Solar UVB-albedo of various surfaces, *Photochem. Photobiol*., *48*, 85–88, 1988.

Bojkov, R., L. Bishop, W. J. Hill, G. C. Reinsel, and G. C. Tiao, A statistical trend analysis of revised Dobson total ozone data over the Northern Hemisphere, *J. Geophys. Res*., *95*, 9785–9807, 1990.

Booth, G. E., T. B. Lucas, T. Mestechkina, J. R. Tusson IV, D. A. Neuschuler, and J. H. Morrow, *NSF Polar Programs UV Spectroradiometer Network 1993–1994 Operating Report*, 203 pp., prepared for Antarct. Support Assoc. and the Natl. Sci. Found. by Biospherical Instrum., San Diego, Calif., 1995.

Chandrasekhar, S., *Radiative Transfer*, 393 pp., Dover, Mineola, N. Y., 1950.

Chou, M.-D., and K.-T. Lee, Parameterization for the absorption of solar radiation by water vapor and ozone, *J. Atmos. Sci*., *53*, 1203–1208, 1996.

Eck, T. F., P. K. Bhartia, P. H. Wang, and L. L. Stowe, Reflectivity of Earth's surface and clouds in ultraviolet from satellite observations, *J. Geophys. Res*., *92*, 4287–4296, 1987.

Eck, T. F., P. K. Bhartia, and J. B. Kerr, Satellite estimation of spectral UVB irradiance using TOMS derived ozone and reflectivity, *Geophys. Res. Lett*., *22*, 611–614, 1995.

Falcone, V. J., W. A. Leonard, and E. P. Shettle, Atmospheric attenuation of millimeter and submillimeter waves: Models and computer code, *AFGL Tech. Rep*., *AFGL-TR-0253*, Air Force Geophys. Lab., Bedford, Mass., 1979.

Farman, J. C., B. G. Gardiner, and J. D. Shanklin, Large losses of total ozone in Antarctica reveal seasonal ClO_x No_x interaction, *Nature*, *315*, 207–210, 1985.

Forster, P. M. de F., Modeling ultraviolet radiation at the Earth's surface, I, The sensitivity of ultraviolet irradiances to atmospheric changes, *J. Appl. Meteorol*., *34*, 2412–2425, 1995.

Forster, P. M. de F., K. P. Shine, and A. R. Webb, Modeling ultraviolet radiation at the Earth's surface, II, Model and instrument comparison, *J. Appl. Meteorol*., *34*, 2426–2439, 1995.

Frederick, J., and D. Lubin, The budget of biologically active ultraviolet radiation in the Earth-atmosphere system, *J. Geophys. Res*., *93*, 3825–3832, 1988.

Fröhlich, C., and J. London, Revised instruction manual on radiation instruments and measurements, *WMO Tech. Note 149*, World Meteorol. Organ., Geneva, Switzerland, 1986.

Herman, J. R., and D. Larko, Low ozone amounts during 1992 and 1993 from Nimbus-7 and Meteor-3 total ozone mapping spectrometers, *J. Geophys. Res*., *99*, 3483–3496, 1994.

Herman, J. R., P. K. Bhartia, J. Ziemke, Z. Ahmad, and D. Larko, UV-B radiation increase (1979–1992) from decreases in total ozone, *Geophys. Res. Lett*., *23*, 2117–2120, 1996.

Herman, J. R., P. K. Bhartia, O. Torres, and C. Hsu, C. Seftor, and E. Celarier, Global distribution of UV-absorbing aerosol from Nimbus-7/TOMS data, *J. Geophys. Res*., *102*, 16,911–16,922, 1997.

Hsu, N. C., J. R. Herman, P. K. Bhartia, C. J. Seftor, O. Torres, A. M. Thompson, J. F. Gleason, T. F. Eck, and B. N. Holben, Detection of biomass burning smoke from TOMS measurements, *Geophys. Res. Lett*., *23*, 745–748, 1996.

Kerr, J. B., and C. T. McElroy, Evidence for large upward trends of ultraviolet-B radiation linked to ozone depletion, *Science*, *262*, 1032–1034, 1993.

King, M. D., Y. J. Kaufman, W. P. Menzel, and D. Tanre, Remote sensing of cloud, aerosol, and water vapor properties, *IEEE Trans. Geosci. Remote Sens*., *30*, 2–27, 1992.

Kneizys, F. X., G. P. Anderson, E. P. Shettle, W. O. Gallery, L. W. Abreu, J. E. A. Selby, J. H. Chetwynd, and S. A. Clough, User's guide to LOWTRAN 7, *AFGL Tech. Rep*., *AFGL-TR-88-0177*, Air Force Geophys. Lab., Bedford, Mass., 1988.

Krotkov, N. A., P. K. Bhartia, J. R. Herman, V. Fioletov, and J. Kerr, Satellite estimation of spectral surface UV irradiance in the presence of tropospheric aerosols, 1, Cloud-free case, *J. Geophys. Res*., *103*, 8779–8793, 1998.

Li, Z., and Louis Moreau, A New Approach for Remote Sensing of Canopy-Absorbed Photosysthetically Active Radiation, I, Total Surface Absorption, *Remote Sens. Environ*., *55*, 175–191, 1996.

Li, Z., H. G. Leighton, K. Masuda, and T. Takashima, Estimation of SW flux absorbed at the surface from TOA reflected flux, *J. Clim*., *6*, 317–330, 1993.

Liou, K. N., A numerical experiment on Chandrasekhar's discrete-ordinate-method for radiative transfer: Applications to cloudy and haze atmosphere, *J. Atmos. Sci*., *30*, 1303–1326, 1973.

Lubin, D., and J. H. Frederick, The ultraviolet radiation environment of Antarctica: McMurdo Station during September–October 1987, *J. Geophys. Res*., *94*, 8491–9496, 1989.

Lubin, D., and E. H. Jensen, Effects of clouds and stratospheric ozone depletion on biologically active ultraviolet radiation trends, *Nature*, *377*, 710–713, 1995.

Madronich, S., Implications of recent total atmospheric ozone measurements for biologically active ultraviolet radiation reaching the Earth's surface, *Geophys. Res. Lett*., *19*, 37–40, 1992.

McKenzie, R. L., M. Kotkamp, and W. Ireland, Upwelling UV spectral irradiances and surface albedo measurement at Lauder, New Zealand, *Geophys. Res. Lett*., *23*, 1757–1760, 1996.

McPeters, R. D., S. M. Hollandsworth, L. E. Flynn, J. R. Herman, and C. J. Seftor, Long-term ozone trends derived from the 16-year combined Nimbus 7/Meteor 3 TOMS Version 7 record, *Geophys. Res. Lett*., *23*, 3699–3702, 1996.

Molina, L. T., and M. J. Molina, Absolute absorption cross section of ozone in the 185- to 350-nm wavelength range, *J. Geophys. Res*., *91*, 14,501–14,508, 1986.

Qu, J., Global ozone and solar ultraviolet-B radiation detection using remote sensing, 163 pp., Ph.D. dissertation, Colo. State Univ., 1997.

Reinsel, G. C., G. C. Tiao, S. K. Ahn, M. Pugh, S. Basu, J. J. Deluisi, C. L. Mateer, A. J. Miller, P. S. Connell, and D. J. Wuebbles, An analysis of the 7-year record of SBUV satellite ozone data: Global profile features and trends in total ozone, *J. Geophys. Res*., *93*, 1689–1703, 1988.

Schwander, H., P. Koepke, and A. Ruggaber, Uncertainties in modeled UV irradiance due to limited accuracy and availability of input data, *J. Geophys. Res*., *102*, 9419–9429, 1997.

Solomon, S., The mystery of the Antarctic ozone "hole," *Rev. Geophys*., *26*, 131–148, 1988.

Stamnes, K., S. C. Tay, W. J. Wiscombe, and K. Jayweera, Numerically stable algorithm for discrete-ordinate-method radiative transfer in multiple scattering and emitted media, *Appl. Opt*., *27*, 2502–2509, 1988.

Stamnes, K., J. R. Slusser, M. Bowen, C. Booth, and T. Lucas, Biologically effective ultraviolet radiation, total ozone abundance, and cloud optical depth at McMurdo station, Antarctic September 15, 1998 through April 15, 1989, *Geophys. Res. Lett*., *17*, 2181–2184, 1990.

Stamnes, K., J. R. Slusser, and M. Bowen, Derivation of total ozone abundance and cloud effects from spectral irradiance measurement, *Appl. Opt*., *30*, 4418–4426, 1991.

Stolarski, R., G. J. Lablow, and R. D. McPeters, Spring time Antarctic total ozone measurements in the early 1970s from the BUV instrument on Nimbus 4, *Geophys. Res. Lett*., *24*, 591–594, 1997.

Tsay, S., and K. Stamnes, Ultraviolet radiation in the Arctic: The impact of potential ozone depletions and cloud effects, *J. Geophys. Res*., *97*, 7829–7840, 1992.

Wang, P., and J. Lenoble, Comparison between measurements and modeling of UV-B irradiance for clear sky: A case study, *Appl. Opt*., *33*, 3964–3971, 1994.

Wang, P., Z. Li, D. I. Wardle, and J. Kerr, Validation of an UV inversion algorithm using satellite and surface measurements, *J. Geophys. Res*., this issue.

Wardle, D. I., E. W. Hare, D. V. Barton, and C. T. McElroy, The world ozone and ultraviolet radiation data centre, paper presented at the Quandrennial Ozone Symposium, l'Aquila, Italy, September 1996.

Wardle, D. I., J. B. Kerr, C. T. McElroy, and D. R. Francis, A Canadian perspective on the changing ozone layer, in *Ozone Science*, 119 pp., Environ. Can., Dartmouth, N. S., 1997.

World Climate Program (WCP), A preliminary cloudless standard atmosphere for radiation computation, *WCP-112*, Assoc. for Meteorol. and Atmos. Phys. Radiat. Comm., 1986.

World Meteorological Organization (WMO), *Scientific Assessment of Stratospheric Ozone: 1989*, *WMO Rep. 30*, Global Ozone Res. and Monit. Proj., Geneva, Switzerland, 1994.

Zeng, J. R., R. L. McKenzie, K. Stamnes, M. Wineland, and J. Rosen, Measured UV spectra compared with discrete ordinate method simulation, *J. Geophys. Res*., *99*, 23,019–23,030, 1994.

J. Cihlar, Z. Li, and P. Wang, Canada Centre for Remote Sensing, 588 Booth Street, Ottawa, Canada, K1A 0Y7.

(Received November 4, 1998; revised February 17, 1999;
accepted February 18, 1999.)